IOPscience iopscience.iop.org

Home Search Collections Journals About Contact us My IOPscience

Crystallized Ohmic Contact Effect in AlGaN/GaN High Electron Mobility Transistor

This content has been downloaded from IOPscience. Please scroll down to see the full text.

2013 Jpn. J. Appl. Phys. 52 081001

(http://iopscience.iop.org/1347-4065/52/8R/081001)

View the table of contents for this issue, or go to the journal homepage for more

Download details:

IP Address: 140.113.38.11
This content was downloaded on 25/04/2014 at 09:16

Please note that terms and conditions apply.

Japanese Journal of Applied Physics 52 (2013) 081001 **REGULAR PAPER**
http://dx.doi.org/10.7567/JJAP.52.081001

Crystallized Ohmic Contact Effect in AlGaN/GaN High Electron Mobility Transistor

Sheng Yu Liao[1], Tsu Chang[2], Hsiao-Hsuan Hsu[3], Chun-Hu Cheng[4]*,
Liann-Be Chang[1], Chin-Pao Cheng[4], and Tun-Chien Teng[4]

[1]*Department of Electronic Engineering, Chang Gung University, Taoyuan 33302, Taiwan, R.O.C.*
[2]*Chung-Shan Institute of Science and Technology, Taoyuan 32544, Taiwan, R.O.C.*
[3]*Department of Electronic Engineering, National Chiao Tung University, Hsinchu 30010, Taiwan, R.O.C.*
[4]*Department of Mechatronic Technology, National Taiwan Normal University, Taipei 10610, Taiwan, R.O.C.*
E-mail: chcheng@ntnu.edu.tw

Received April 1, 2013; accepted May 25, 2013; published online July 18, 2013

In this study, we investigate the grain size effect of high electron mobility transistor devices with ohmic contact metals of stacked Ti/Al/Ni/Au and Ti/Al/Mo/Au. In addition to a comparison of electrical characteristics, the ohmic contacts were also examined by a scratch test for the observation of adhesion behavior. The experimental results demonstrate that the metal grain size is strongly dependent on metal adhesion, which may lead to bonding issues. Moreover, the grain-induced lateral stress lowers the drive current and increases the off-state current owing to the degraded gate swing and transconductance of transistor switching characteristics. © 2013 The Japan Society of Applied Physics

1. Introduction

The AlGaN/GaN high-electron mobility transistor (HEMT) has been widely investigated for microwave power devices and circuits owing to its wider band gap, larger breakdown voltage, and higher saturation velocity than GaAs.[1–7] To obtain good high-frequency characteristics, the gate length scaling, channel carrier density, and interface traps should be taken into consideration.[8–12] Furthermore, the crystallization effect of the ohmic contact is important to lower the contact resistance and improve the device reliability for RF applications. The ohmic contact of Ti/Al/Ni/Au is one of the commonly used schemes for AlGaN/GaN HEMT devices. However, the use of a Ni barrier with poor thermal stability also brings issues regarding device uniformity and reliability. The Mo barrier has a high melting point; therefore, a stacked Ti/Al/Mo/Au was proposed. According to previous studies,[13,14] Ti/Al/Mo/Au metallization with small surface roughness and low contact resistance has been realized,[15–18] but the adhesive properties and corresponding device characteristics have been less discussed. In this study, we investigate the crystallization effect in an AlGaN/GaN HEMT device with stacked metals of Ti/Al/Ni/Au and Ti/Al/Mo/Au to provide a comprehensive study from the local crystallization effect to the output transistor characteristics. An apparent correlation was found between crystallization size and device performance on the basis of different ohmic contact schemes. This study can offer in-depth understanding of the ohmic contact process including the effects of metal crystallization and alloy inter diffusion. It is helpful to clarify the influence of leakage currents originating from the defect state around the AlGaN surface and the two-dimensional electron gas (2DEG) channel.

2. Experimental Procedure

First, AlGaN/GaN heterostructures were grown on sapphire substrates by metal organic chemical vapor deposition (MOCVD). The epitaxial structure consists of a 2-μm-thick unintentionally doped GaN buffer layer and a 20-nm-thick $Al_{0.25}GaN_{0.75}N$ barrier layer. The electron sheet charge density and hall mobility of the HEMT structure were $>1 \times 10^{13}\,cm^{-2}$ and $1900\,cm^2\,V^{-1}\,s^{-1}$, respectively. After mesa etching for isolation, ohmic contact metals were formed using the evaporated Ti/Al/Ni/Au and Ti/Al/Mo/Au stacks and followed by an 850 °C annealing for 30 s in N_2 ambient. After ohmic contact formation, the 1 μm mushroom-shaped gate of Ni metal was defined. Low-cost Ni featuring a high work function of 5.1 eV and good thermal stability has been used in dynamic random access memory (DRAM) devices.[19–22) Finally, the passivation layer was covered to reduce the amount of surface defects on the AlGaN barrier layer. The adhesion properties of ohmic contact metals were analyzed using a nanoscratch measurement system.[23–25]

3. Results and Discussion

Figures 1(a) and 1(b) show the drain current-to-drain voltage (I_d–V_d) and drain current-to-gate voltage (I_d–V_g) characteristics, respectively, of AlGaN/GaN HEMT devices fabricated using different contact metals of Ti/Al/Ni/Au and Ti/Al/Mo/Au. Similar drive currents of 80 mA/mm are obtained in both devices with different contact metals. However, the AlGaN/GaN device with the Ti/Al/Mo/Au contact exhibits a lower off-state current than that with the Ti/Al/Ni/Au contact. The large off-state current of >0.1 mA/mm and small on–off ratio of $<10^3$ are 10× higher than those of the Ti/Al/Mo/Au contact. Since the source and drain activation is critical to decreasing the contact resistance, the transistor characteristics are influenced by surface morphology and metal alloyed diffusion after high temperature annealing. Figure 2(a) shows the X-ray diffraction (XRD) analysis of annealed Ti/Al/Ni/Au and Ti/Al/Mo/Au contacts. The TiAl peak gives evidence of a reactor with AlGaN and the large peak of the AlNi alloy indicates the consumption of a large number of Ni atoms. The consumption of the Ni barrier would result in the poor blocking effect owing to inter diffusion of uncontrolled metal alloys in Ti/Al/Ni/Au. Furthermore, the Ni–Al alloy aggregation in some local areas may form bulges resulting in a higher surface roughness.[26] On the other hand, the peaks of $GaMo_3$ alloys detected in Ti/Al/Mo/Au are attributed to the low solubility of Mo-rich particles in Al and Au.[15] The formation of alloyed screw dislocations via $GaMo_3$ results in conductive paths to the 2DEG[27] that can effectively lower the contact resistance.

In Fig. 2(b), the atomic force microscope (AFM) topogram with a $5 \times 5\,\mu m^2$ scan of the contact metal surface shows

 © 2013 The Japan Society of Applied Physics

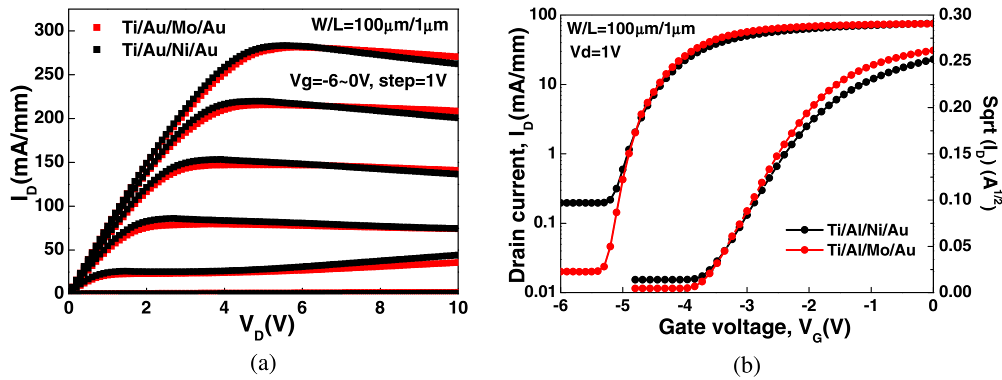

Fig. 1. (Color online) (a) I_d–V_d and (b) I_d–V_g characteristics of AlGaN/HEMT devices with Ti/Al/Ni/Au and Ti/Al/Mo/Au ohmic contacts.

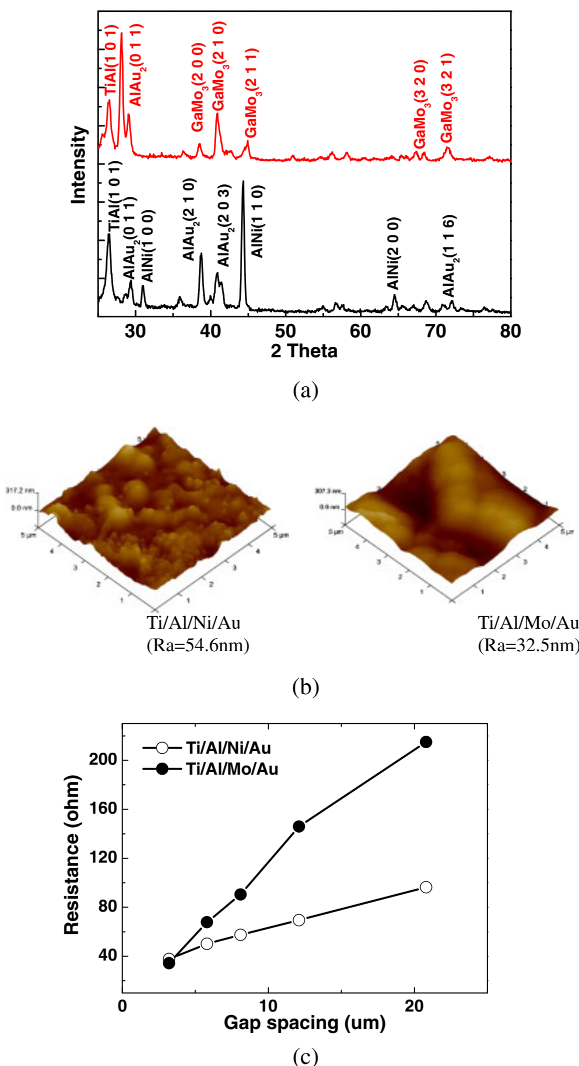

Fig. 2. (Color online) (a) XRD spectra, (b) AFM images, and (c) specific contact resistances of AlGaN/HEMT devices with Ti/Al/Ni/Au and Ti/Al/Mo/Au ohmic contacts.

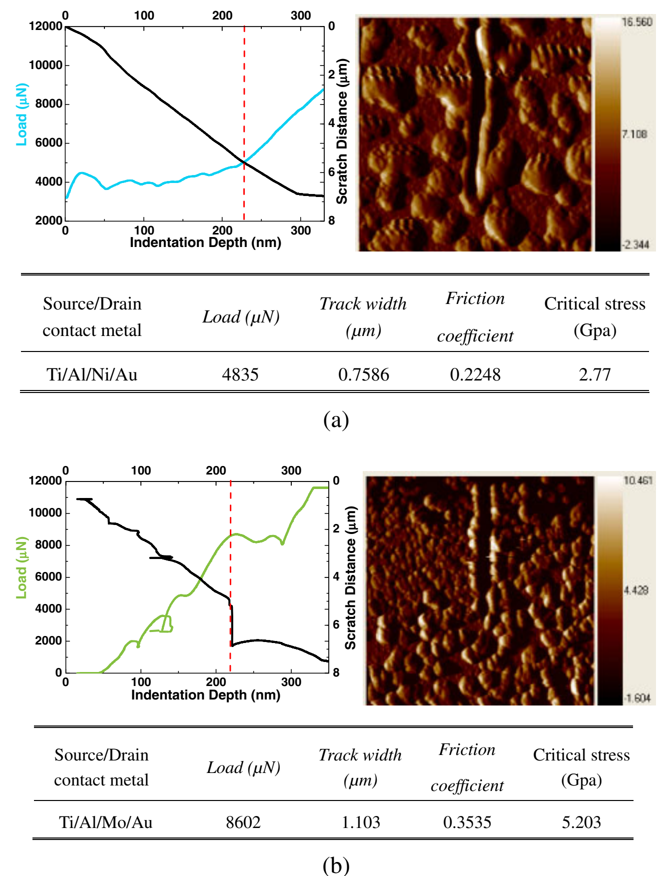

Source/Drain contact metal	*Load (μN)*	*Track width (μm)*	*Friction coefficient*	Critical stress (Gpa)
Ti/Al/Ni/Au	4835	0.7586	0.2248	2.77

(a)

Source/Drain contact metal	*Load (μN)*	*Track width (μm)*	*Friction coefficient*	Critical stress (Gpa)
Ti/Al/Mo/Au	8602	1.103	0.3535	5.203

(b)

Fig. 3. (Color online) Load–indentation depth curves of Ti/Al/Ni/Au and Ti/Al/Mo/Au ohmic contacts. The critical load and stress have been extracted, as shown in the following tables for comparison.

different surface roughness for both annealed contact metals. We can observe that the root-mean-square (rms) of 54.6 nm on the Ti/Al/Ni/Au surface is much larger than that on the Ti/Al/Mo/Au surface. The rough surface can result in unwanted gate leakage due to the formation of surface traps near the Schottky gate. As shown in Fig. 2(c) measured from the transmission line pattern (TLM), the extracted specific contact resistances for Ti/Al/Ni/Au and Ti/Al/Mo/Au contacts are 8×10^{-5} and $1.5 \times 10^{-6}\,\Omega\,\mathrm{cm}^2$, respectively. The above results reveal that the contact resistances are also affected by surface morphology and metal crystallization. Thus, the Ti/Al/Mo/Au metal contact shows the advantages of the low contact resistance, small grain size, and smooth surface morphology that are also beneficial for improving the gate leakage and on–off current ratio.

To study this issue, we conduct a scratch test on annealed contact metals, as shown in Figs. 3(a) and 3(b). We observe that the contact loadings are different for these metal

 © 2013 The Japan Society of Applied Physics

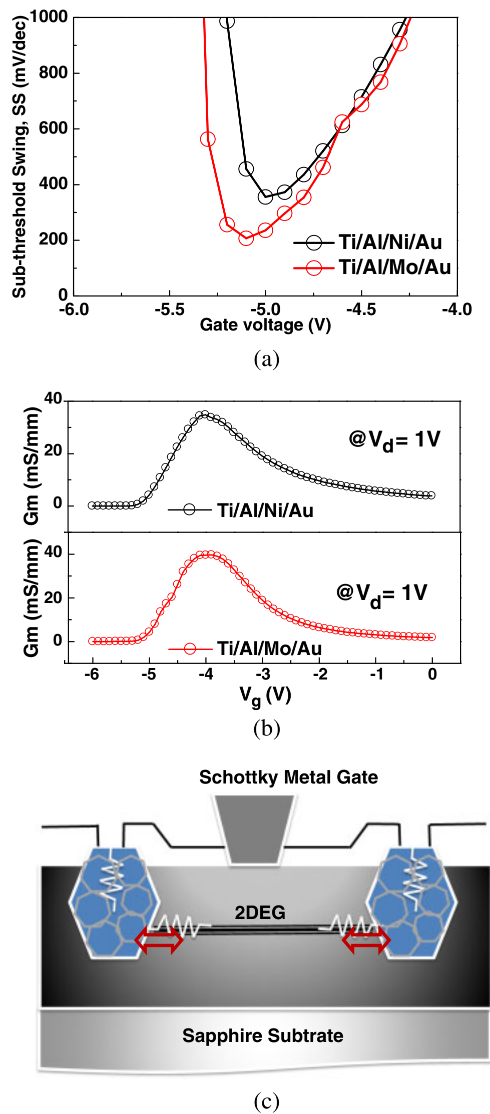

Fig. 4. (Color online) (a) Sub threshold swing, (b) transconductance, and (c) schematic plot of AlGaN/HEMT devices with Ti/Al/Ni/Au and Ti/Al/Mo/Au ohmic contacts.

surfaces. For the Ti/Al/Ni/Au contact, the applied loading shows an abrupt increase in the initial stage, which is mainly ascribed to the rough surface with large crystal grains (Al–Ni alloy grains). Subsequently, the accumulated scratch process is in situ monitored using an AFM tool with an increase in applied load. After finishing the scratch test, the friction coefficients calculated from the ratio of the scratch force to the normal load are obtained. The friction force is also dependent on the interfacial shear stress; therefore, the friction coefficient cannot be considered as a constant in the scratch test, especially for multi layer structures.

The large friction coefficient obtained for the Ti/Al/Mo/Au surface indicates a large shear stress and a good adhesion properly that simultaneously correspond to a small track width, as shown in the right AFM images. Also, the much larger grain size on the Ti/Al/Ni/Au surface is clearly observed by AFM. Compared with the critical stress (5.2 GPa) of the Ti/Al/Mo/Au contact, the lower stress of 2.77 GPa demonstrates that the adhesion of the contact metal is greatly influenced by the grain size of the crystallized alloy. The poor surface adhesion would cause a large ground inductance owing to the bonding issue, which can lower the RF power gain. Moreover, a non uniform strain induced by local stress due to the large grain size would affect the output characteristics of the HEMT device.

To further investigate the effect of grain size in contact metals, we extract the sub-threshold swing (*SS*) characteristic of HEMT devices, as shown in Fig. 4(a). The *SS* is linked to trap densities near the interface or channel.[28–30] We can find that the *SS* (355 mV/decade) of Ti/Al/Ni/Au is much higher than that (206 mV/decade) of Ti/Al/Mo/Au. The increase in the *SS* property or threshold voltage could be attributed to the large off-state current, implying an increase in power consumption. In Fig. 4(b), the degraded *SS* is also supported by the low transconductance (G_m), suggesting that the transistor switching behavior is related to the charge density near the channel. Therefore, the 12% degraded G_m is believed to be attributable to carrier trapping via grain boundaries or strain relaxation of the 2DEG channel [Fig. 4(c)]. The large grains with high grain boundary defects allow the occurrence of electron trapping and in turn affect the carrier transport in the 2DEG channel under an on-state current. In other words, the grains of the metal contact with a multi alloy not only result in bonding issues such as poor adhesion and a large bonding wire inductance, but also affect the *SS* and G_m of transistor switching characteristics.

4. Conclusions

In this study, we investigate the grain size effect of HEMT devices with ohmic contact metals of stacked Ti/Al/Ni/Au and Ti/Al/Mo/Au. After high-temperature activation, the multi alloy contact with a large grain size in Ti/Al/Ni/Au not only leads to bonding issues such as poor adhesion and a large bonding wire inductance, but also seriously affects the gate swing and transconductance of transistor switching characteristics.

1) S. J. Pearton, J. C. Zolper, R. J. Shul, and F. Ren: J. Appl. Phys. **86** (1999) 1.
2) S. Keller, Y.-F. Wu, G. Parish, N. Zhang, J. J. Xu, B. P. Keller, S. P. DenBaars, and U. K. Mishra: IEEE Trans. Electron Devices **48** (2001) 552.
3) Y. Ando, Y. Okamoto, H. Miyamoto, T. Nakayama, T. Inoue, and M. Kuzuhara: IEEE Electron Device Lett. **24** (2003) 289.
4) Y.-F. Wu, A. Saxler, M. Moore, R. P. Smith, S. T. Sheppard, P. M. Chavarkar, T. Wisleder, U. K. Mishra, and P. Parikh: IEEE Electron Device Lett. **25** (2004) 117.
5) S. T. Sheppard, K. Doverspike, W. L. Pribble, S. T. Allen, J. W. Palmour, L. T. Kehias, and T. J. Jenkins: IEEE Electron Device Lett. **20** (1999) 161.
6) Y.-F. Wu, D. Kapolnek, J. P. Ibbetson, P. Parikh, B. P. Keller, and U. K. Mishra: IEEE Trans. Electron Devices **48** (2001) 586.
7) C. Y. Tsai, T. L. Wu, and A. Chin: IEEE Electron Device Lett. **33** (2012) 35.
8) S. Yagi, M. Shimizu, H. Okumura, H. Ohashi, Y. Yano, and N. Akutsu: Jpn. J. Appl. Phys. **46** (2007) 2309.
9) C. Poblenz, P. Waltereit, S. Rajan, S. Heikman, U. K. Mishra, and J. S. Speck: J. Vac. Sci. Technol. B **22** (2004) 1145.
10) D. S. Lee, X. Gao, S. Guo, and T. Palacios: IEEE Electron Device Lett. **32** (2011) 617.
11) C. H. Cheng, T. Chang, S. Y. Liao, H. M. Chang, W. D. Ho, Y. C. Shiau, and J. S. Sen: 222nd Meet. Electrochemical Society, 2012, p. 2544.
12) C. H. Cheng, T. Chang, S. Y. Liao, W. D. Ho, Y. C. Shiau, J. S. Sen, and H. M. Chang: 222nd Meet. Electrochemical Society, 2012, p. 2940.

© 2013 The Japan Society of Applied Physics

13) R. Vetury, N. Q. Zhang, S. Keller, and U. K. Mishra: IEEE Trans. Electron Devices **48** (2001) 560.
14) P. B. Klein, J. A. Freitas, S. C. Binari, and A. E. Wickenden: Appl. Phys. Lett. **75** (1999) 4016.
15) L. Wang, F. M. Mohammed, and I. Adesida: Appl. Phys. Lett. **87** (2005) 141915.
16) Y. Sun, X. Chen, and L. F. Eastman: J. Appl. Phys. **98** (2005) 053701.
17) J. Gillespie, A. Crespo, R. Fitch, G. Jessen, and G. Via: Solid-State Electron. **49** (2005) 670.
18) M. W. Fay, G. Moldovan, P. D. Brown, I. Harrison, J. C. Birbeck, B. T. Hughes, M. J. Uren, and T. Martin: J. Appl. Phys. **92** (2002) 94.
19) C. H. Cheng, H. C. Pan, H. J. Yang, C. N. Hsiao, C. P. Chou, S. P. McAlister, and A. Chin: IEEE Electron Device Lett. **28** (2007) 1095.
20) C.-H. Cheng, K.-C. Chiang, H.-C. Pan, C.-N. Hsiao, C.-P. Chou, S. P. McAlister, and A. Chin: Jpn. J. Appl. Phys. **46** (2007) 7300.
21) C. H. Cheng, S. H. Lin, K. Y. Jhou, W. J. Chen, C. P. Chou, F. S. Yeh, J. Hu, M. Hwang, T. Arikado, S. P. McAlister, and A. Chin: IEEE Electron Device Lett. **29** (2008) 845.
22) C.-C. Huang, C.-H. Cheng, B.-H. Liou, F.-S. Yeh, and A. Chin: Jpn. J. Appl. Phys. **48** (2009) 081401.
23) H.-C. Wen, C.-S. Yang, and W.-C. Chou: Appl. Surf. Sci. **256** (2010) 2128.
24) H.-C. Wen, C.-I. Hung, H.-J. Tsai, C.-K. Lu, Y.-C. Lai, and W.-K. Hsu: J. Mater. Chem. **22** (2012) 13747.
25) B.-C. He, C.-H. Cheng, H.-C. Wen, Y.-S. Lai, P.-F. Yang, M.-H. Lin, W.-F. Wu, and C.-P. Chou: Microelectron. Reliab. **50** (2010) 63.
26) R. Gong, J. Wang, S. Liu, Z. Dong, M. Yu, C. P. Wen, Y. Cai, and B. Zhang: Appl. Phys. Lett. **97** (2010) 062115.
27) D. Selvanathan, F. M. Mohammed, A. Tesfayesus, and I. Adesida: J. Vac. Sci. Technol. B **22** (2004) 2409.
28) H.-H. Hsu, C.-Y. Chang, and C.-H. Cheng: Phys. Status Solidi: Rapid Res. Lett. **7** (2013) 285.
29) C. H. Cheng, K. I. Chou, and A. Chin: Solid-State Electron. **82** (2013) 111.
30) M. A. Khan, X. Hu, G. Sumin, A. Lunev, J. Yang, R. Gaska, and M. S. Shur: IEEE Electron Device Lett. **21** (2000) 63.

© 2013 The Japan Society of Applied Physics